Composites Part C: Open Access 8 (2022) 100291

Contents lists available at ScienceDirect

Composites Part C: Open Access

journal homepage: www.sciencedirect.com/journal/composites-part-c-open-access

On the thermal and mechanical performance of Polycarbonate / Titanium Nitride nanocomposites in material extrusion additive manufacturing

N. Vidakis [a], M. Petousis [a], N. Mountakis [a], S. Grammatikos [b,*], V. Papadakis [c], J.D. Kechagias [d], S.C. Das [b]

[a] Department of Mechanical Engineering, Hellenic Mediterranean University, Heraklion 71410, Greece
[b] Laboratory for Advanced and Sustainable Engineering Materials (ASEMlab), Department of Manufacturing and Civil Engineering, Norwegian University of Science and Technology, Gjøvik 2815, Norway
[c] Institute of Molecular Biology and Biotechnology, Foundation for Research and Technology – Hellas, Heraklion, 71110, Greece
[d] School of Technology, University of Thessaly, Karditsa 43100, Greece

ARTICLE INFO

Keywords:
Three-dimensional (3D) printing
Fused filament fabrication (FFF)
Nanocomposites
Polycarbonate (PC)
Titanium nitride (TiN)
Mechanical characterization

ABSTRACT

The development of cost-effective multipurpose nanocomposites with a superior mechanical response is of key importance in a variety of industries, such as the ones in the aircraft and the medical field. Such enhancement contributes to the reduction of the weight and dimensions of the part, which are critical parameters for the design. To achieve that, herein, Titanium Nitride (TiN) in nanopowder form was used as an enhancement agent for the Polycarbonate (PC) polymer. Nanocomposites were fabricated with Fused Filament Fabrication (FFF), which is a Material Extrusion (MEX) 3D printing process. The aim was to evaluate the effect of the additive in the polymeric matrix, in an effort to produce superior filaments for demanding applications. Samples were produced, to be assessed for conforming to the corresponding standards, as well as to be characterized regarding their mechanical, thermal, and spectroscopic responses. The impact of the filler concentration was also considered. Their morphological characteristics were documented via Atomic Force Microscopy (AFM), as well as Scanning Electron Microscopy (SEM). It is found that the introduction of the TiN nanopowder acts as an enhancement of the matrix material's mechanical properties. The nanocomposite with 3 percent weight-to-weight (wt.%) additive concentration exhibited overall the most enhanced mechanical response. The processability and the thermal properties of the Polycarbonate matrix were kept almost intact, making the process easily upgradable for industrial use.

1. Introduction

Polycarbonate (PC) is a common thermoplastic polymer that is utilized in a variety of applications, including aircraft and trains [1], optical applications [2, 3], membranes [4], photovoltaics [5], and medical applications [6]. This is mainly due to its superior mechanical and aging performance, making it one of the most commonly used polymers [1]. Research for the PC polymer is related to its mechanical properties, such as its impact strength [7], the improvement of its mechanical response, with the addition of suitable fillers and the development of composites [8, 9], its stability as a polymer [10], and the improvement of its physical properties, such as its flammability [1], that will further expand its fields of applications. As expected, its performance in Additive Manufacturing (AM) is a popular research topic in the literature, in material extrusion (MEX) [11] and inkjet printing [12]. The aim is to improve and optimize its performance for acoustic [13], bio-based [14], and manufacturing [15] applications, among others. Research in the field is focusing on the effect of the 3D printing parameters on the mechanical properties of the PC polymer [11, 16, 17], while computational [18] and statistical modeling tools have also been employed to optimize the process [19]. Such tools are commonly used in MEX to optimize the process [20, 21]. The thermal performance of the 3D printed parts is also critical for specific types of applications and has been reported in the literature [22]. For the improvement of its properties and to induce a multi-functional behavior, that will further expand its fields of application, composites have been developed, using PC as the matrix material, with various fillers [23–25], showing strong potential for use in different industrial and medical applications. The addition of fillers for

* Corresponding author.
E-mail address: sotirios.grammatikos@ntnu.no (S. Grammatikos).

https://doi.org/10.1016/j.jcomc.2022.100291

Available online 29 June 2022

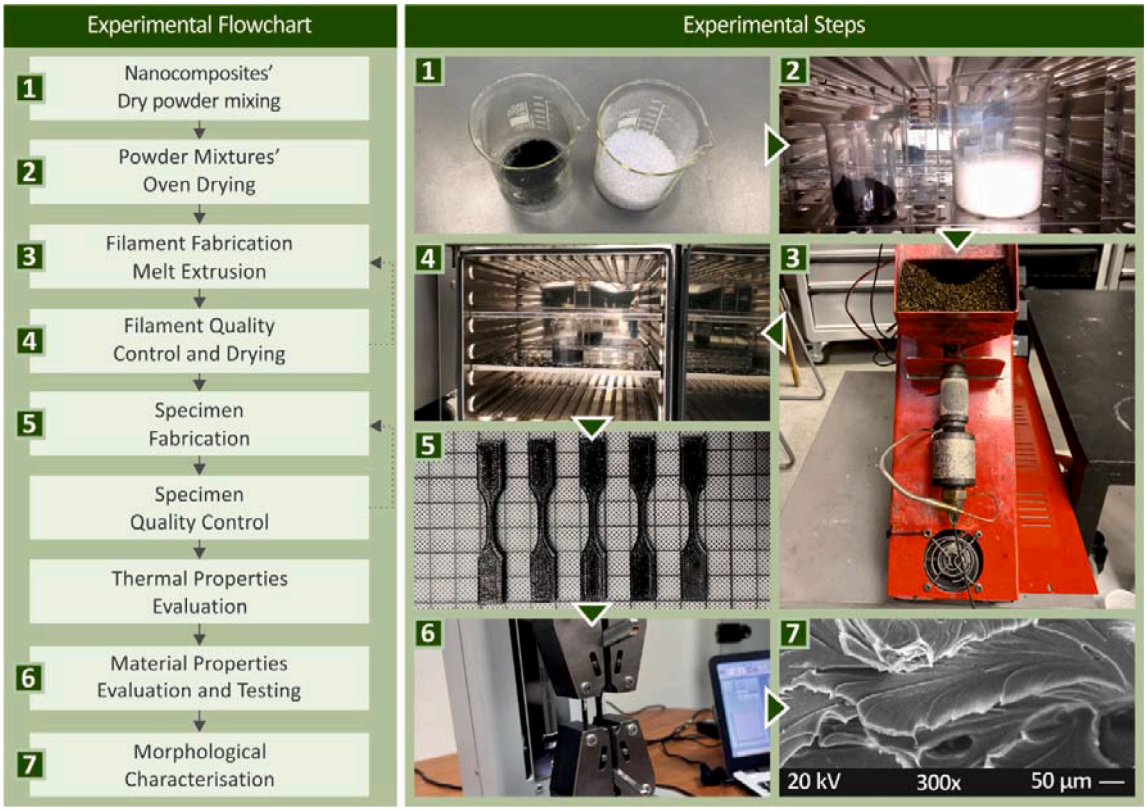

Fig. 1. Current study process.

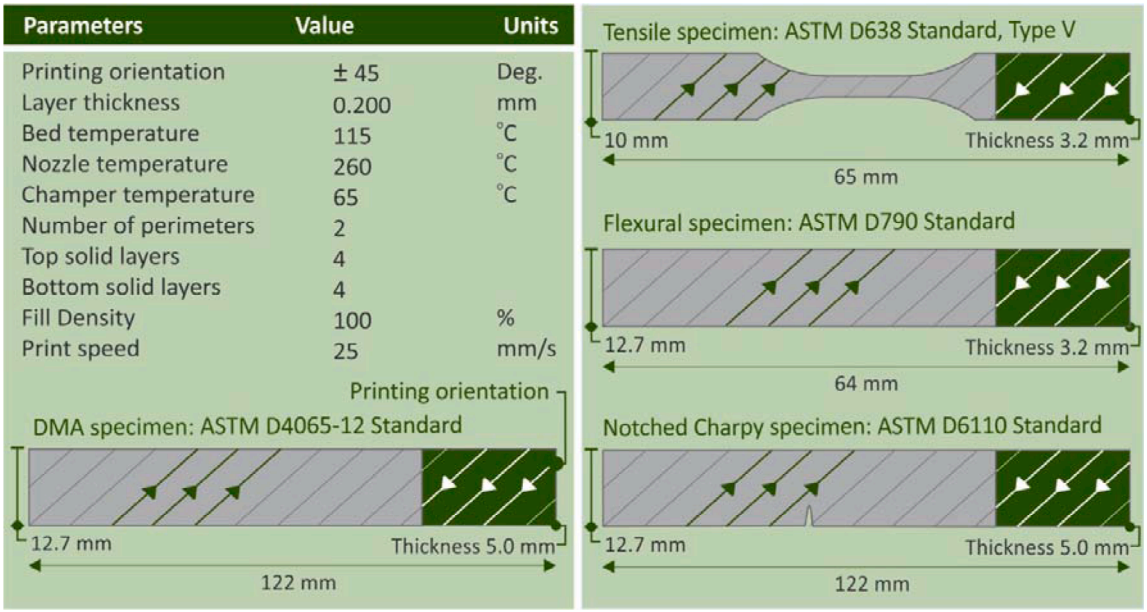

Fig. 2. Settings for the fabrication of the specimens of this work with 3D printing. On the right side of the figure, the manufactured specimens' dimensions are presented.

the improvement of the final part performance is a common approach in the literature [26–33]. Additionally, design approaches for multi-materials components have also been presented in the literature [34]. The effect of introducing different materials in AM, on the manufacturability and metrics has also been investigated [35].

Titanium nitride (TiN) is a material used in various applications. It is widely used in coatings for increasing the wear resistance of surfaces [36–38], in medical implants [39] and energy applications [40], as a shield for electromagnetic interference [41], and atmosphere control [42], and in optical applications [43–47], mainly due to its temperature depended on optical properties. Although it is widely used in applications, in AM its use is still limited. Research in the field is focusing again on AM for coatings [48], metal medical implants [49], and optical applications [50]. TiN has been applied as a coating to PC for bio-electrode

Table 1
Mechanical characterization tests.

DMA	
Test	Three-point-bending
Range of Temperature	30–200 °C
Rate of Temperature	5 °C/min
Oscillation magnitude	30 μm
Frequency	1 Hz
Preload	0.1 N
Standard	ASTM D4065–12
Device	TA Instruments, model DHR 20 (TA Instruments, New Castle, DE, USA)
Tensile	
Samples	Type V (3.2 mm thickness)
Strain rate	10 mm/min
Standard	ASTM D638–02a
Device	Imada, model MX2 (Northbrook, IL, USA)
Flexural	
Type of test	Three-point-bending
Span length	52 mm
Strain rate	10 mm/min
Standard	ASTM D790
Device	Imada, model MX2 (Northbrook, IL, USA)
Impact	
Type of test	Charpy
Samples	Notched
Release height	367 mm
Standard	ASTM D6110
Device	Terco, model MT 220 (Kungens Kurva, Sweden)
Microhardness	
Method	Vickers
Applied load	200 gF
Indentations' duration	10s
Standard	ASTM E384–17
Device	Innova Test, model 300 (Maastricht, The Netherlands)

applications [51] and as a hardening coating [52]. No research has been presented so far utilizing TiN as a filler in the PC polymer, let alone in AM or 3D printing.

In this work, TiN in nanoparticles (NPs) form was introduced to the PC polymer matrix and nanomaterials were developed at various filler concentrations, suitable for 3D printing with the MEX process. The aim was to prepare nanocomposites with improved mechanical properties, which are in high demand nowadays in AM since they contribute to the expansion of the fields of application of the process. In this direction, for the first time, the effect of TiN as an enhancement agent in the PC polymer was investigated, with the nanocomposites prepared in a form suitable for MEX 3D printing. The feasibility and the processability of the nanocomposites developed within the contents of this work were also evaluated. As expected, the porosity and the 3D printing structure negatively affect the properties of the materials in the mechanical tests [53]. The improvement of the strength of the materials contributes to the reduction of the parts' weight, and the material consumption, which are essential parameters in the parts' design. The nanomaterials in this work were prepared with a thermomechanical process, which is material extrusion. With this process specimens were then 3D printed confronting mechanical testing international standards. Apart from the mechanical characterization, the morphological characteristics were also investigated with scanning electron microscopy (SEM) and with atomic force microscopy (AFM). The thermal properties were assessed, to confirm that the process implemented herein does not affect the stability of the nanocomposites. To this end, Thermogravimetric Analysis (TGA) and Differential scanning calorimetry (DSC) were employed. Raman analysis was employed to reveal the spectroscopic response of the nanocomposites. The addition of TiN had a positive effect in all cases studied, verifying that it can be applied as a reinforcement additive in the PC polymer. The highest improvement in the mechanical properties was found at the nanocomposite with a 3 percent weight-to-weight TiN concentration (wt.%). This nanomaterial had overall the most enhanced mechanical response. The processability or the thermal properties of the PC polymer were not negatively affected in MEX 3D printing by the filler addition. So, the nanomaterials developed herein are expanding the use of the 3D printing process in applications requiring polymeric materials and at the same time improved mechanical properties.

2. Material and methods

The current study's workflow is depicted in Fig. 1.

2.1. Materials

In this work, nanocomposites were prepared from raw materials. To achieve that, the material extrusion process was employed. The matrix material was PC, procured in pellets form (type EMERGE 8430–15, density 1.20 g/cm^3, tensile strength 70.0 MPa, and maximum strain 110%), from Styron Europe GmbH (Horgen, Switzerland). Titanium

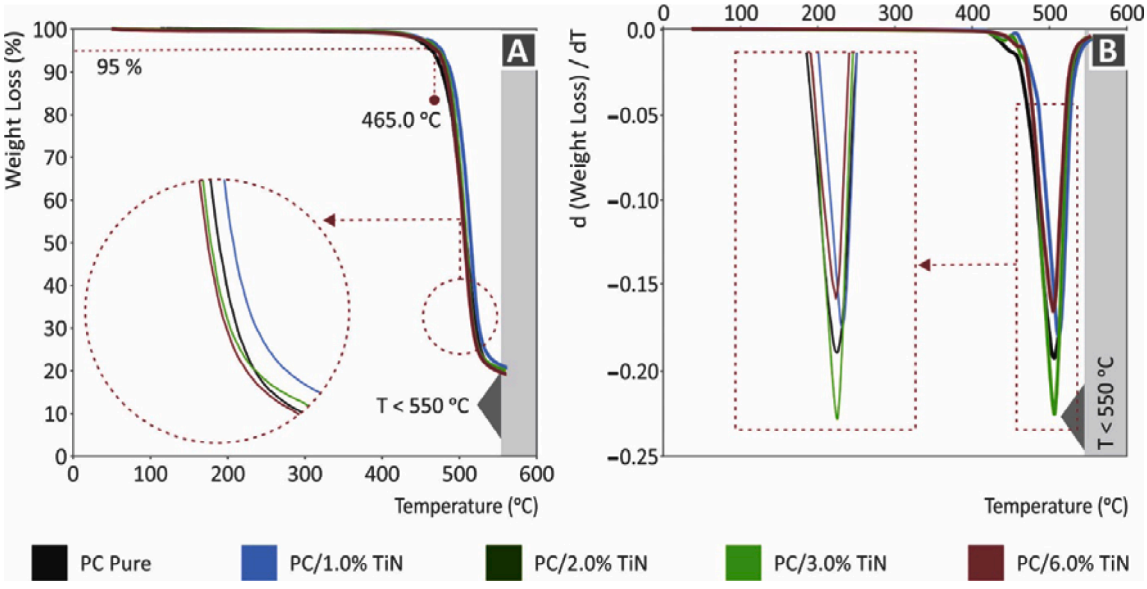

Fig. 3. TGA graphs of the materials tested: (A) weight (%) vs. temperature (°C); (B) mass degradation rate (dw/dT) vs. temperature (°C).

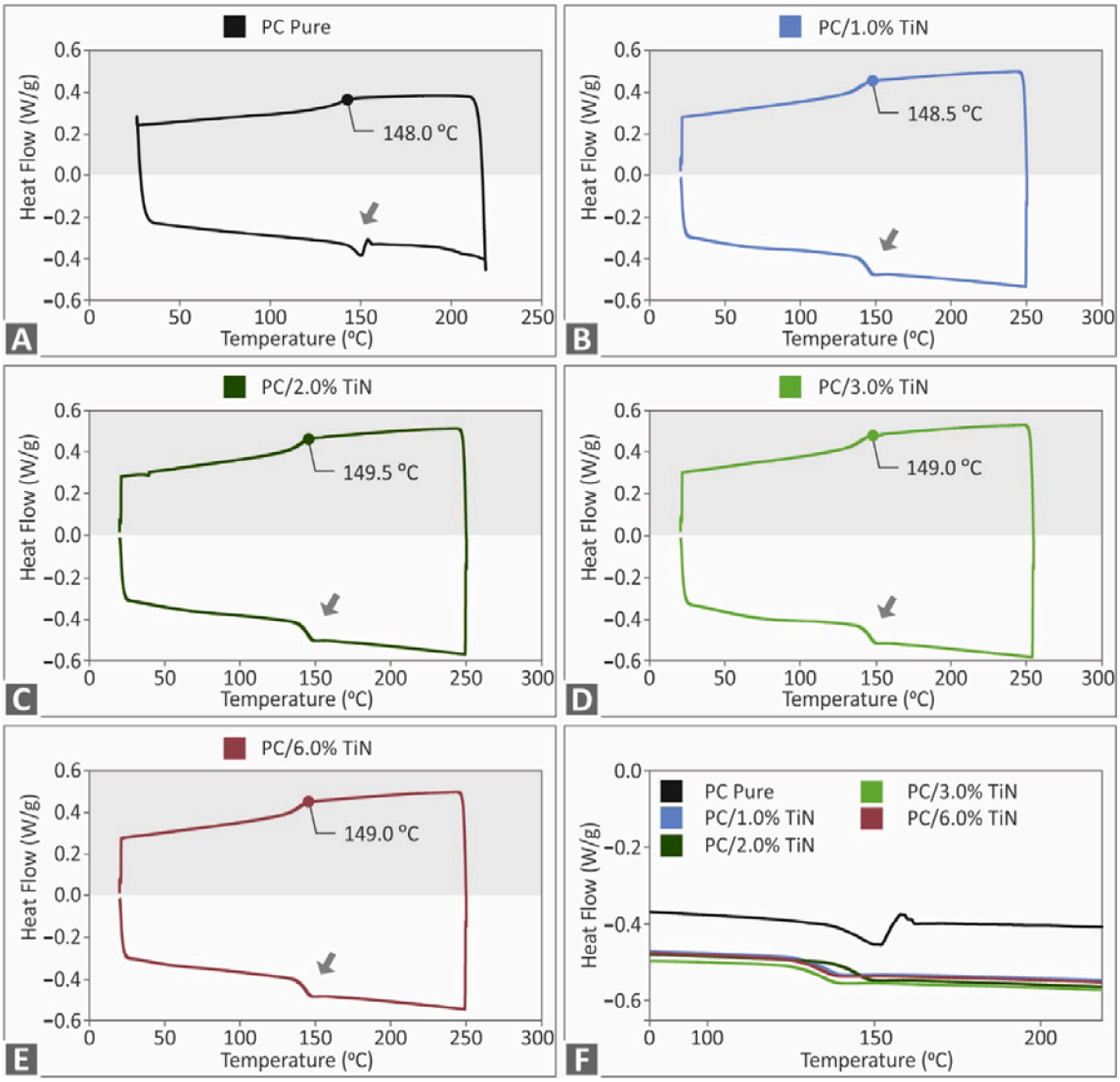

Fig. 4. Exotherm and endotherm heat flow curve (W/g) to temperature (°C) in DSC for PC: (A) pure, (B) with TiN 1 wt.%, (C) with TiN 2 wt.%, (D) with TiN 3 wt.%, (E) with TiN 6 wt.%, and (F) exotherm curves comparison.

nitride (TiN) in nanopowder (purity 99.2+%, size 20 nm, cubic, specific Surface Area 50–80m^2/g, true density 5.3 gr/cm^3, melting point 2950 °C) powder form, sourced from Nanographi (Ankara, Turkey), was used as the additive in the nanomaterials.

2.2. Nanocomposites preparation

Raw materials were initially diverted into nanocomposites in a 1.75 mm diameter filament form suitable for MEX 3D printing (one different filament for each nanocomposite, i.e., filler loading). To this end, raw materials were initially dried to remove any moisture in them. The process was implemented in a laboratory furnace at 60 °C for 24 h. Then, four separate mixtures of the PC polymer and the TiN additive were prepared. Each mixture contained the matrix material and the additive in different weight-to-weight (wt.%) concentration, i.e., 1.0, 2.0, 3.0, and 6.0 wt.%. A high-power blender was used for the mixing process. It was placed in a glove box to restrict the powder spread in the atmosphere. Mixtures were further dried before they were poured into a single screw extruder Noztek (Shoreham-by-Sea, UK). This was necessary for an initial spreading of the additive in the PC polymer. This filament was then diverted into pellets with a 3devo shredder (Utrecht, The Netherlands). With these pellets, filament for MEX 3D printing was then produced in a 3devo Composer (Utrecht, The Netherlands) single screw extruder. This extruder has, according to its manufacturer, a screw geometry specially designed for materials and additives blending. It produces a 1.75 mm diameter filament for MEX 3D printing. Heating zones 1–3 (1 is close to the nozzle) were set at 200 °C, while heating zone 4 was set at 240 °C. The screw was rotating at 4.8 rpm. These conditions were determined experimentally for the materials before the production of the filament for the current work. This process with the two extrusion steps, with the second extruder specially designed for materials mixing, was aiming to improve the dispersion of the additive in the matrix. Pure PC polymer filament was also produced with the extrusion process, from pure PC pellets, without any additives, to fabricate pure PC specimens, for evaluation purposes in the study.

2.3. Specimens manufacturing

With the produced filament in the previous step for all the PC/TiN nanocomposites and pure PC, specimens were manufactured for mechanical testing, according to international standards. A 3D printer sourced from Intamsys, model Funmat HT (Shanghai, China) was employed, with settings determined experimentally for these materials before the fabrication of the specimens of this work (Fig. 2). G-codes

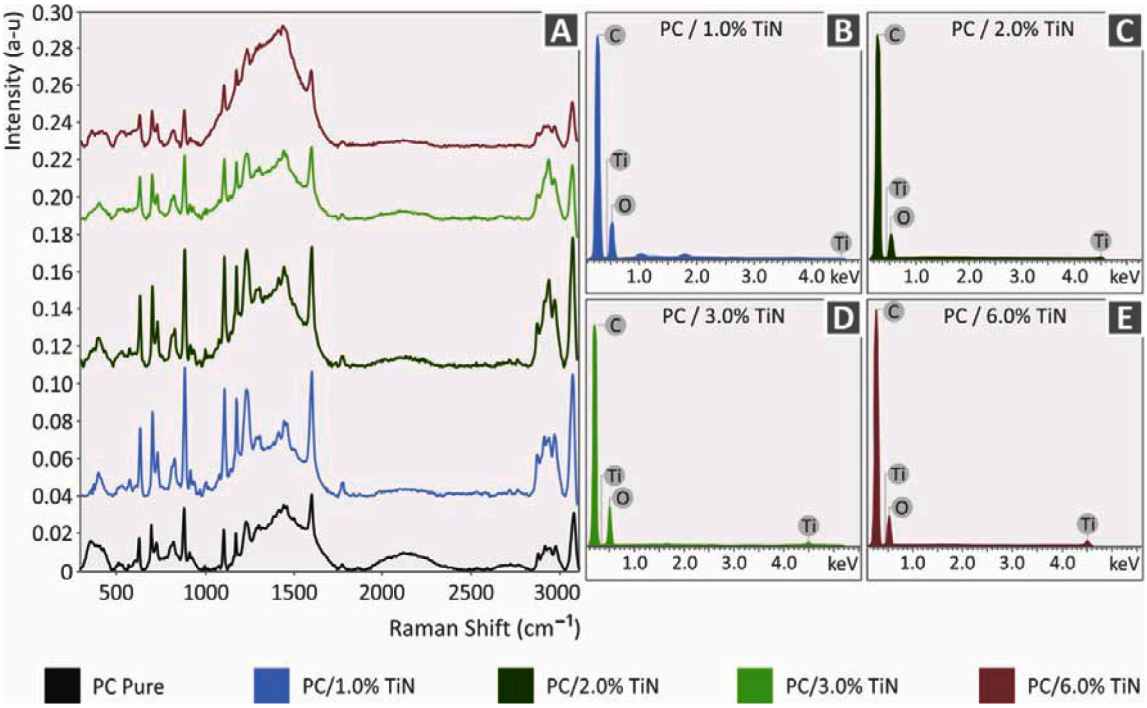

Fig. 5. (A) For the materials tested Raman spectroscopy graphs, (B) EDS for PC/TiN 1 wt.%, (C) EDS for PC/TiN 2 wt.%, (D) EDS for PC/TiN 3 wt.%, and (E) EDS for PC/TiN 6 wt.%.

Table 2
Major Raman peaks identified and their related assignments.

Wavenumber (cm^{-1})	Raman peak assignment
573	Phenyl ring vibration
633	phenyl ring vibration
703	C-H out-of-plane bending
731	C—H out-of-plane bending
826	phenyl ring vibration
886	ν[O−(C = O)−O], ν(C−CH3), τ(CH3), ν(ring)
1109	C-O-C stretching
1176	C—O—C stretching
1234	C-O-C group asymmetric vibration
1602	phenyl ring vibration
2874	$CH_2\nu_S$ or C—H
2912	$CH_2\nu_{AS}$ or C—H
2971	CH/CH_2 stretch modes polarized
3073	C-H stretching

were prepared with the Intamsuite software platform (Shanghai, China). Five specimens were manufactured for each mechanical test, following the corresponding standard (Fig. 2). The 3D printing parameters values were experimentally determined, before the manufacturing of the samples for this work. A similar approach for parameter selection is proposed in the literature [54].

2.4. Thermal and spectroscopic properties

The thermal properties of the materials were investigated using TGA and DSC, to evaluate the temperatures employed in the extrusion process and the materials' thermal stability. The spectroscopic reaction of the materials was also revealed by Raman's investigations. TGA was performed in a Perkin Elmer Diamond apparatus (Waltham, MA, USA) (temperature cycle 40 °C to 550 °C, temperature step 10 °C/min, a Nitrogen atmosphere). DSC was performed in a TA Instruments DSC 25 apparatus (New Castle, DE, USA) (temperature cycle 25–225–25 °C, 5 min at 225 °C, step 15 °C/min).

A modified LabRAM HR Raman Spectrometer (HORIBA Scientific, Kyoto, Japan) was used to perform Raman spectroscopy on the samples. The microscope is based on a 532 nm central wavelength solid-state laser module, with a 90 W maximum laser output power. The microscopic objective lens used had a magnification of 50 × and a numerical aperture of 0.5. It had a long working distance of 10.6 mm (LMPlanFL N, Olympus) and was used to deliver the excitation light and collect the Raman signals. On the sample, the laser spot had dimensions of proximately 1.7 μm laterally, and 2 μm axially. The power of the laser was controlled through a neutral density (ND) filter. In this experiment, 5% of laser light was allowed to go through, which resulted in 2 mW power on the samples. The spectrometer used 600 groves grating resulting in a spectral resolution of ~ 2 cm^{-1}. To acquire the 300 to 3100 cm^{-1} Raman spectral range, the microscope had to use two optical windows or two acquisitions for every point. The acquisition time used was 10 s with five accumulations per measurement. LabSpec 6 (HORIBA Scientific, Kyoto, Japan) was used to process all Raman Spectra. The processing steps started by removing the background using an internal function based on polynomial fit. In the next step, data were normalized using Unit Vector for a better comparison between the samples.

2.5. Filament evaluation

Before the fabrication of the 3D printed specimens, the filament was evaluated for its diameter, its tensile strength, and its surface morphological characteristics. The diameter was measured using the extruder's closed-loop real-time diameter measuring system and manual measurements in random spots with a high-quality caliper. Tensile tests were performed using an Imada MX2 tensile test instrument (Northbrook, IL, USA). To fix the filament in the instrument during the experiments, custom grips were developed. The findings of the tensile tests can also be used to assess the impact of the 3D printing process on materials. Using AFM, the morphological properties of the filament's side surface were studied. The microscope used was a MicroscopeSolver P47H Pro (Moscow, Russia) (300 kHz resonant frequency). The effect of the filler on the morphological form is related to the quality of the filaments produced.

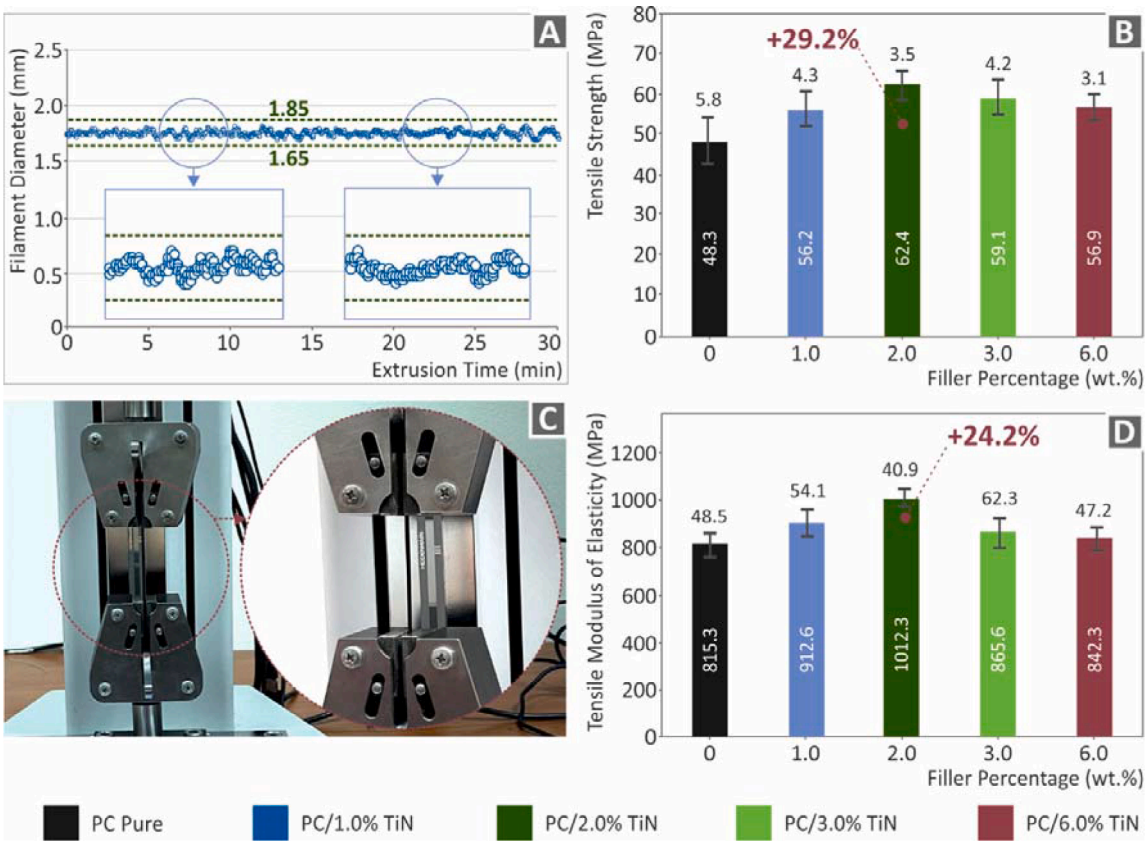

Fig. 6. Filament evaluation for all materials tested: (A) Monitoring of the diameter during the filament production, (B) mean tensile strength values and deviation calculated for the five samples tested, (C) experimental setup of the tensile tests for the filament, and (D) mean values and deviation calculated for the five samples tested for the modulus of elasticity calculated in the tensile experiment.

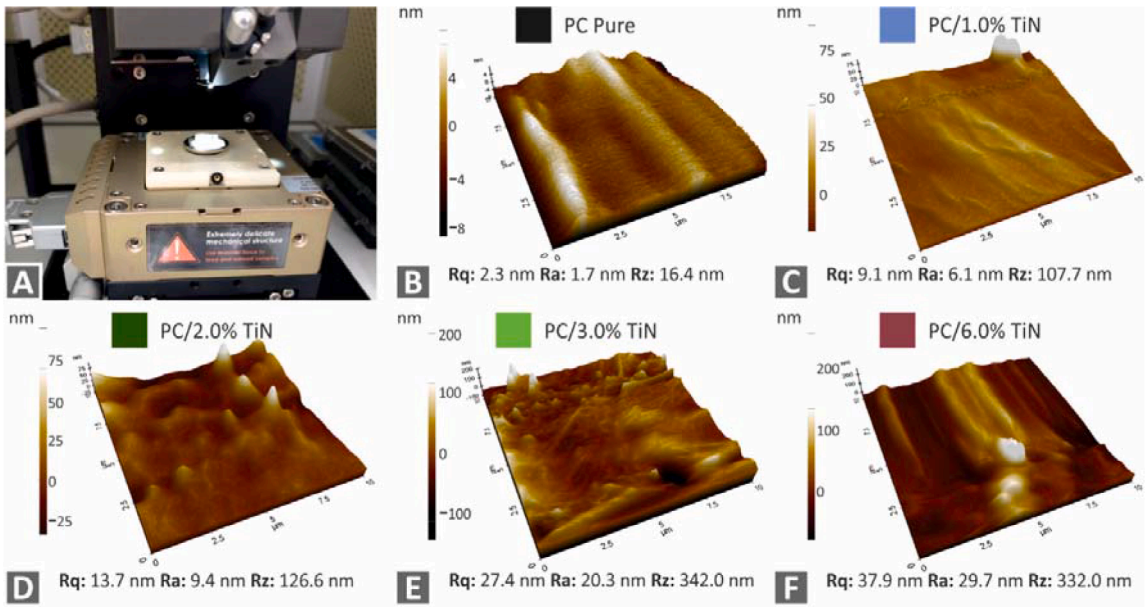

Fig. 7. Filament surface morphology evaluation employing AFM: (A) experimental setup, and PC (B) pure, with TiN (C 1 wt.%, (D) 2 wt.%, (E) 3 wt.%, and (F) 6 wt.%.

2.6. Mechanical characterization

The tests performed and their parameters for the characterization of the nanocomposites' mechanical properties are listed in Table 1 below. The tests were performed at room temperature.

2.7. Characterization of the morphology of the specimens

The characterization of the 3D printed specimens' morphology assessed the specimens' 3D printing quality (by examining the side surface of the specimens) as well as their fracture mechanism in tensile

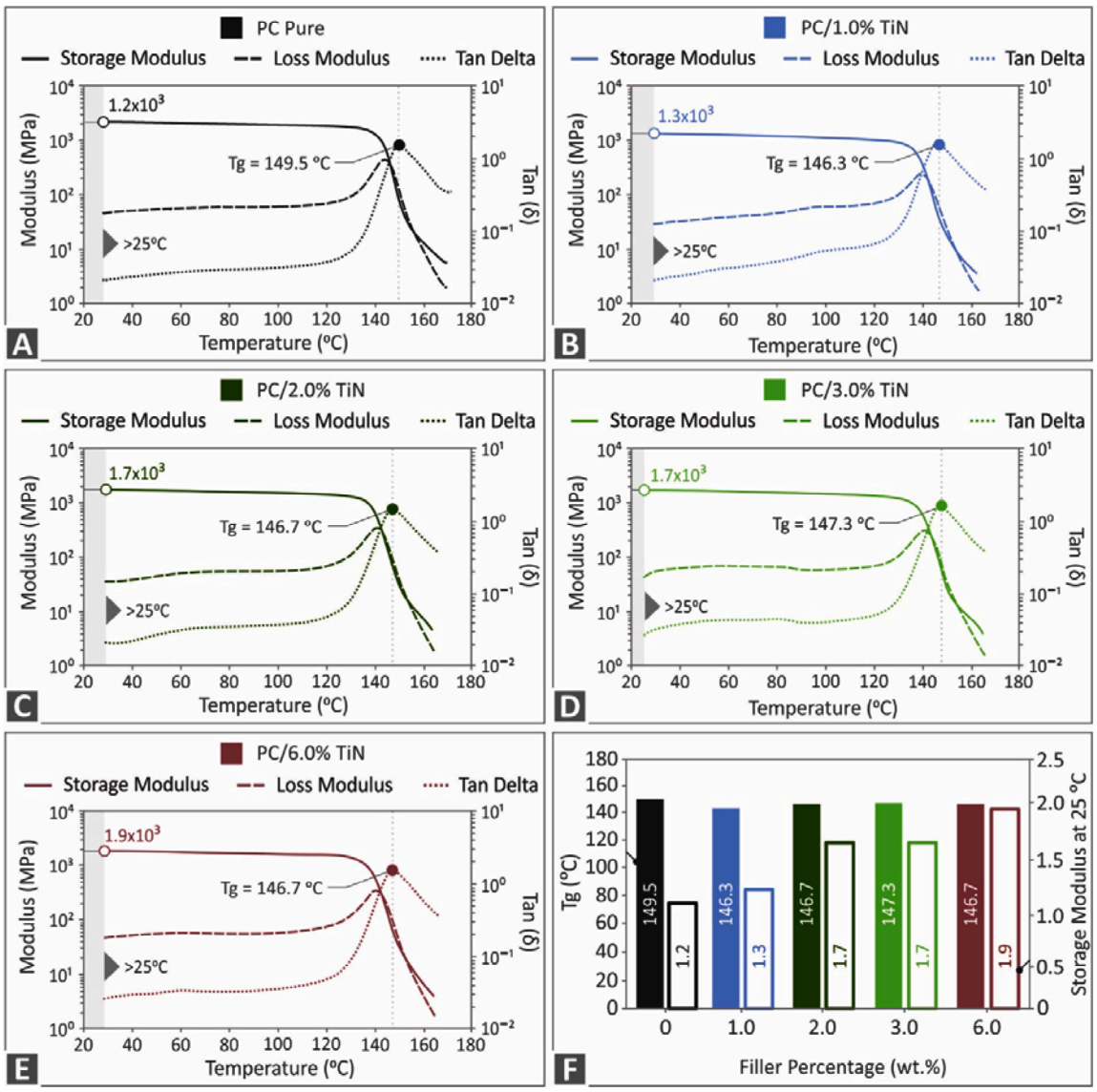

Fig. 8. Results on the DMA tests (Storage modulus, loss modulus, and tan(delta)), PC: (A) pure, and with TiN (B) 1 wt.%, (C) 2 wt.%, (D) 3 wt.%, (E) 6 wt.%, and (F) at 25 °C, calculated glass transition temperature values Tg (°C) and calculated storage modulus values.

tests. Scanning electron microscopy (SEM) images were obtained in high-vacuum mode on a JEOL JSM 6362LV (Peabody, MA, USA) (20 kV). Gold-sputtered specimens were used. The elements in the nanocomposites were also verified by energy dispersive x-ray analysis (EDX). Specimens were not coated in this case.

3. Results

3.1. Thermal properties and spectroscopic analysis

The weight loss vs temperature curves, derived from the TGA, are presented in Fig. 3. As it is shown, the addition of the filler does not significantly affect the thermal behavior of the pure polymer material. The intense weight loss starts at about 465 °C for all the materials assessed. This verifies that the temperatures employed in the study for material extrusion are not in a range that affects the thermal behavior of the materials. The maximum weight loss rate occurred at about the same temperature for all materials (Fig. 3b). The 3 wt.% loading showed the maximum weight loss rate. No trend was observed connecting these parameters to the filler loading. The weight loss over temperature and the respective weight loss over time graphs for the nanocomposites studied herein, provide valuable information about the thermal properties of the produced materials. Additionally, they confirm that the addition of the filler in the matrix does not compromise the thermal stability of the matrix material. The corresponding DSC curves are presented in Fig. 4. In all cases, a similar response is observed, with the addition of the filler having no important effect on the material's characteristic temperatures. The only significant discovery was that adding the filler enhanced the absorbed energy in both the endotherm and exotherm phases, with changes with filler loading being minor.

Fig. 5A shows the Raman spectra graphs for all materials tested. Through the analysis of PC pure, the major Raman peaks were identified, and their related assignments were found in the literature. Raman peaks identified are between the range of 573 cm^{-1} and up to 3073 cm^{-1}. The spectrum measured matched that of polycarbonate [55–58]. The results are presented in Table 2.

3.2. Filament evaluation

The real-time filament diameter values recorded by the filament extruder integrated feature are presented in Fig. 6a. As it is shown, the diameter of the produced filament is with acceptable deviation, making

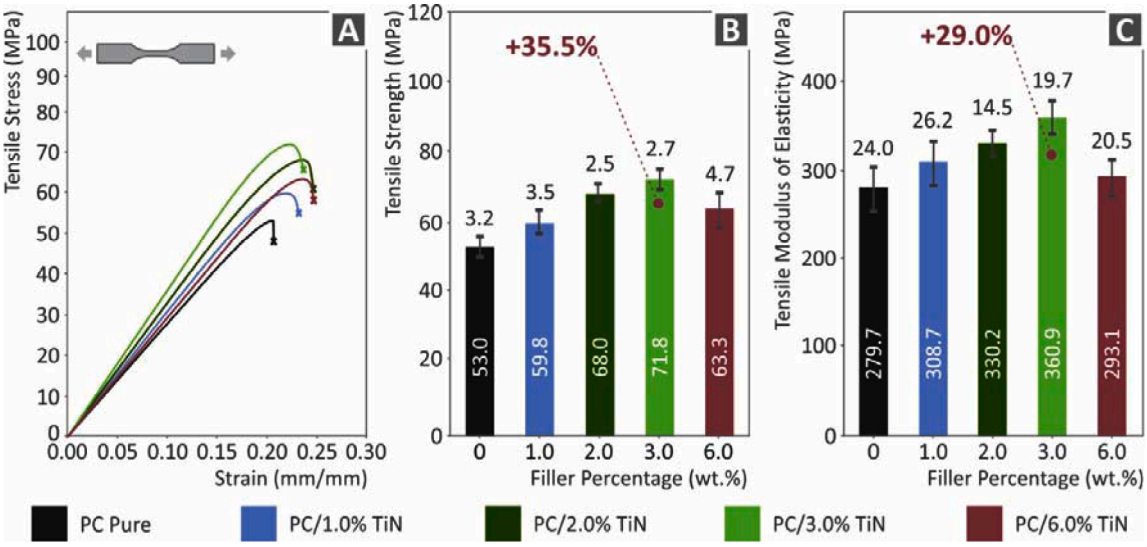

Fig. 9. Tensile experiment results: (A) stress vs. strain curves, (B) average tensile strength and deviation calculated for the five samples tested, and (C) average tensile modulus of elasticity and deviation calculated for the five samples tested.

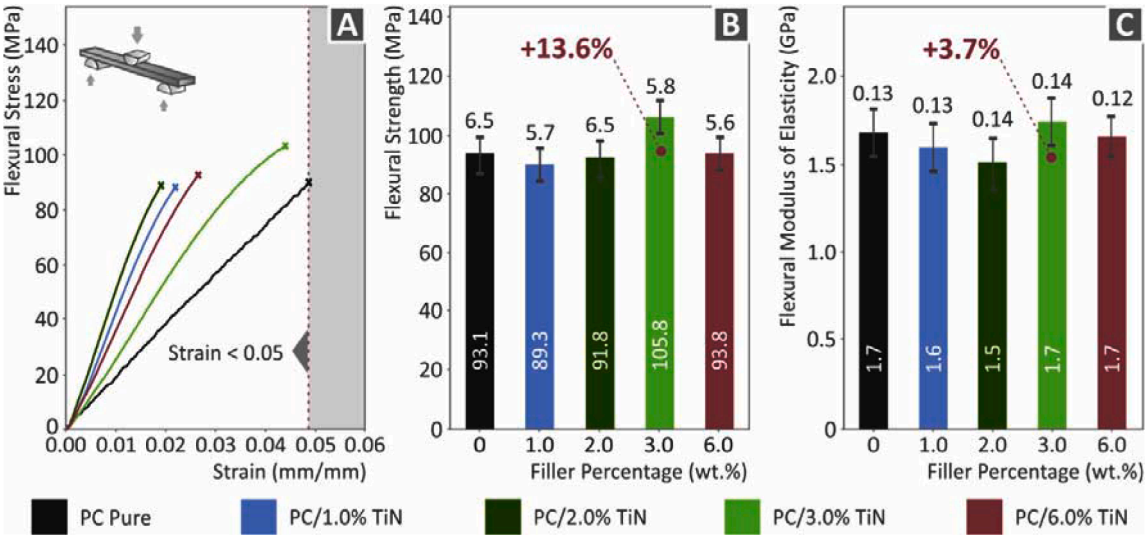

Fig. 10. Flexural experiment graphs (following the standard, the experiment was terminated at 5% strain): (A) stress vs. strain, (B) average flexural strength and deviation calculated for the five samples tested, and (C) average flexural modulus of elasticity and deviation calculated for the five samples tested.

it suitable for MEX 3D printing. Figs. 6b and 6d show the results from the tensile tests of the filament, while Fig. 6c shows the corresponding experimental setup. From the test results, it is reported that the filler addition improves the tensile strength of the pure PC polymer. The highest improvement of a noTable 29.2% was achieved for the nanocomposite with 2 wt.% loading, which also had the highest improvement in its stiffness, about 24.2% higher than the pure PC polymer. In the nanocomposite with 6 wt.% filler concentration, the tensile test values start to decrease, indicating that saturation of the filler is expected by slightly increasing the filler concentration. Still, even at this loading, the response of the nanocomposite is higher than the pure PC polymer. Results from the morphological analysis results of the side surface of the filament acquired with AFM are depicted in Fig. 7. The introduction of the additive in the matrix increases the filament surface roughness, with its values further increasing, when increasing the additive concentration.

3.3. Results of 3D printed specimens' mechanical characterization

DMA test results are depicted in Fig. 8. The addition of the filler has no substantial effect on the material's response, as seen by the graphs, with the curves following a similar pattern. The addition of the filler slightly decreased the glass transition temperature (Tg) of the polymer, with the filler loading having no significant effect on Tg. The Storage Modulus was increasing with the filler concentration increase. Overall, adding the filler did not significantly affect the viscoelastic behavior of the polymer. These results indicate the response of the materials under dynamic loading and different temperature ranges. Such conditions are quite common when using the parts in industrial and real-life environments, so the behavior of the prepared materials under such conditions should be known and is considered critical for the mechanical characterization of the materials.

Fig. 9 shows the tensile experiment outcome obtained in this work. The inclusion of the filler resulted in the polymer being reinforced. In comparison with the pure PC polymer, the tensile test values were raised in all loadings investigated. The nanocomposite with 3 wt.% filler

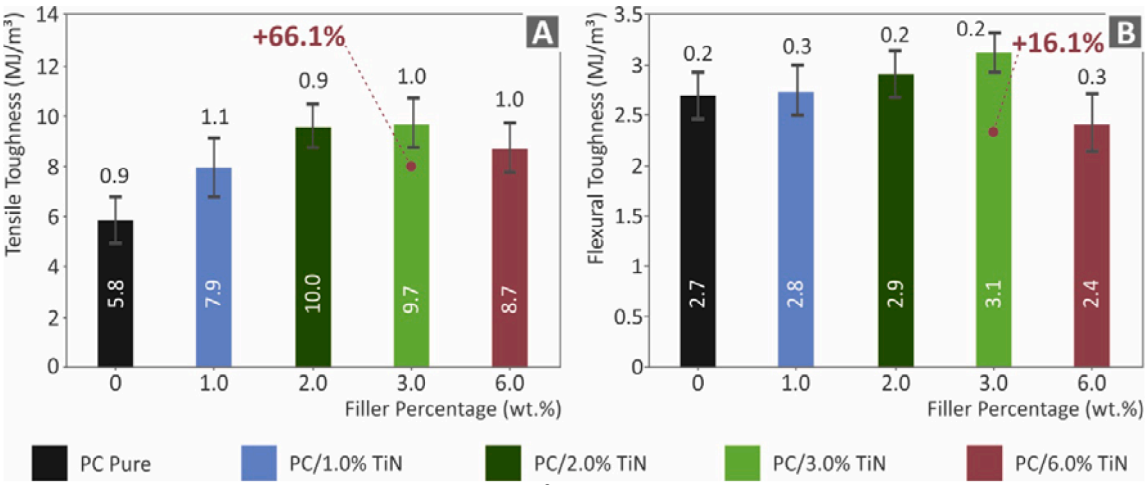

Fig. 11. (A) average tensile toughness (MJ/m^3) and the calculated deviation calculated for the five samples tested, (B) average flexural toughness (MJ/m^3), and the calculated deviation calculated for the five samples tested.

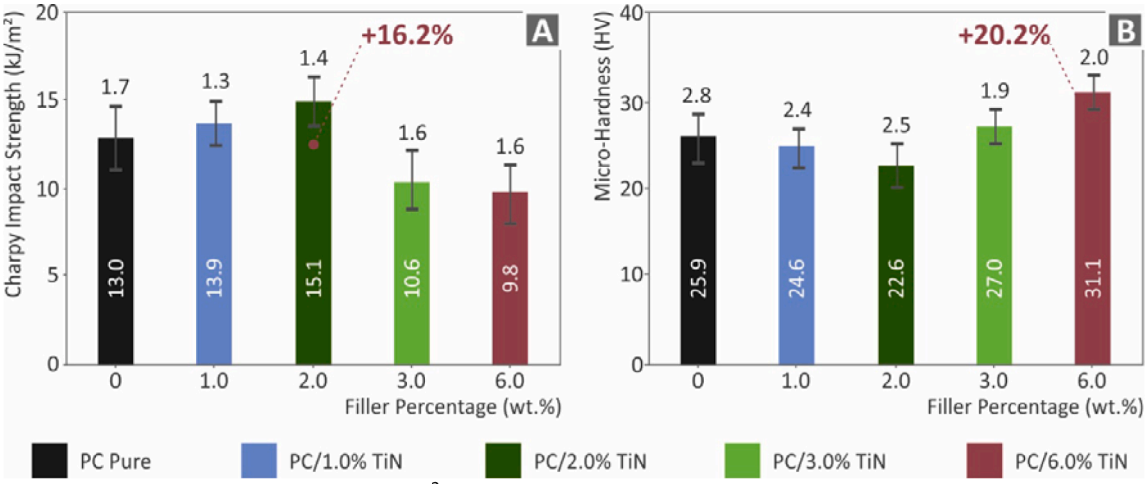

Fig. 12. (A) impact strength (kJ/m^2) and deviation calculated for the five samples tested, (B) Vickers microhardness and deviation calculated for the five samples tested.

concentration had the highest reinforcing, 35.5% more than pure PC. The nanocomposite was also found to be 29% stiffer than pure PC. In tensile testing, the greatest loading of 6 wt.% exhibited a reduced mechanical response, although it showed roughly 20% higher tensile strength than the matrix material. The flexural test results presented in Fig. 10 do not follow the same trends as the tensile tests. The addition of the filler has a negative effect on the flexural strength for loadings up to 2 wt.%. In flexural tests, the 3 wt.% filler concentration results in a 13.6% increase in the response when compared to the corresponding results for the pure PC material and a 3.7% rise in the flexural modulus of elasticity. The flexural test results decrease at the nanocomposite with 6 wt.% additive concentration (the highest loading investigated), compared to the 3 wt.%, but still are marginally increased when compared to the corresponding values of the pure PC polymer. The values for the tensile and the flexural toughness are derived as integrals of the corresponding stress versus strain graphs. These values indicate the amount of energy absorbed by the material during the testing. The calculated average values with their deviations for this work are presented in Fig. 11. As it can be observed, they follow a similar trend to the corresponding strength values. The 3 wt.% loading nanocomposite achieved 66.1% higher values than the pure PC in the tensile toughness and 16.1% in the flexural toughness.

The impact test results do not follow the same trend as the other mechanical tests (Fig. 12). Low filler loadings increase the impact strength of the PC polymer, with the highest enhancement of 16.2% calculated for the nanocomposite with 2 wt.% filler loading. At higher filler concentration nanocomposites showed an inferior response in this test when compared to the corresponding values of the pure PC polymer. Regarding the Vickers microhardness measurements, also the trend of this mechanical property is not similar to the other mechanical characterization tests. When compared to pure PC, the Vickers microhardness values are lower at low filler concentrations. The highest enhancement was recorded for the highest additive concentration nanocomposite of 6 wt.% investigated in this work (20.2% improvement compared to the pure PC material).

3.4. Characterization of the morphology of the specimens

SEM images for pure PC from the side and the fracture surface at two zoom levels are presented in Fig. 13. The fracture surface (Figs. 13a and 13b) shows areas without any deformation in the filament strands, indicating a brittle failure (right side of Fig. 13a), and areas with visible deformation in the filament strands, indicating a more ductile failure (left side of Fig. 13a). The side surface images (Figs. 13c and 13d) show an excellent 3D printing quality without defects or voids and a perfect layer interfusion. This shows that the 3D printing settings employed in

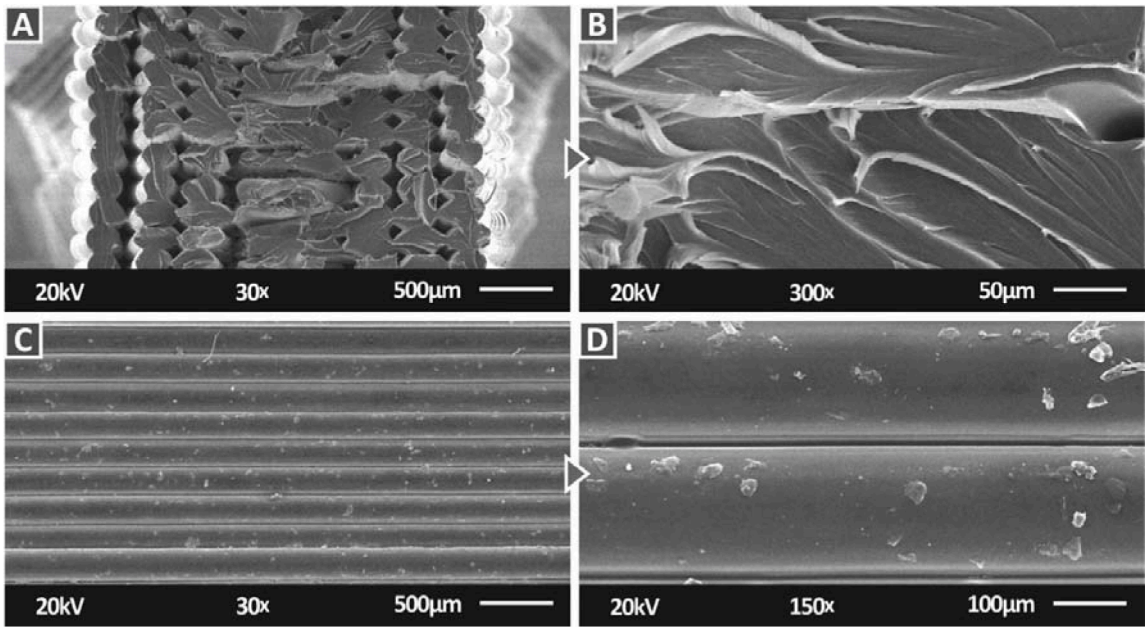

Fig. 13. Pure PC SEM images: (A) fracture surface at a magnification of 30 ×, (B) fracture surface at a magnification of 300 ×, (C) side surface at a magnification of 30 ×, (D) side surface at a magnification of 150 ×.

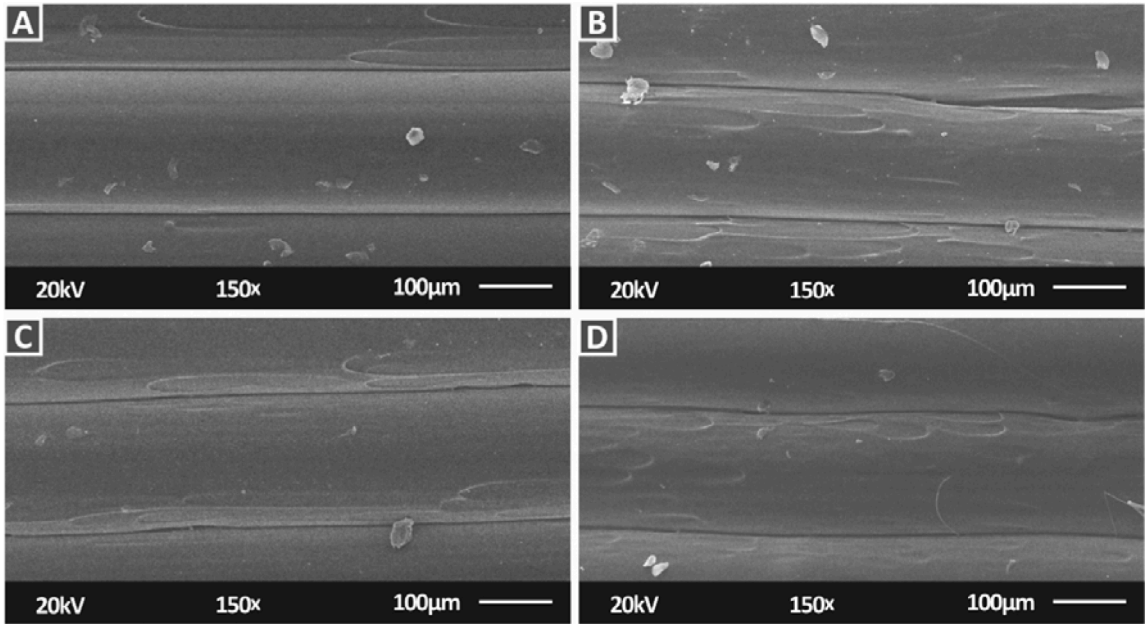

Fig. 14. Side surface of the PC/TiN nanocomposites captured with SEM at 150 × magnification: (A) nanocomposite with 1 wt.% filler concentration, (B) nanocomposite with 2 wt.% filler concentration, (C) nanocomposite with 3 wt.% filler concentration, and (D) nanocomposite with 6 wt.% filler concentration.

the work were the appropriate ones for the material and no processability issues occurred. The same can be concluded from the side surface SEM images of the nanocomposites tested in this work (Fig. 14). The fracture surface of the nanocomposites was inspected also with SEM and images at two magnifications are presented in Fig. 15. At the 1 wt.% loading a ductile response can be observed, with visible deformation of the filament strands (Figs. 15a and 15b). At 2 and 3 wt.% loading, the fracture is ductile with minimum to no deformation observed in the filament strands (Figs. 15c-15f). A mixed fracture surface can be seen at the filler loading of 6 wt.% (the highest concentration studied), with certain strands exhibiting deformation, mostly on the sides of the specimen, and a brittle behavior in the middle with no obvious deformation, demonstrating how the fracture evolved in the specimen in the test. To check the dispersion of the nanoadditive in the PC polymer, SEM images of 5000 × were captured, to examine the materials for possible agglomerations (Fig. 16). In the majority of the cases, no significant agglomerations were discovered. The EDS graph was captured in the specimen with a 3 wt.% filler loading agglomeration area (Fig. 16c). In the EDS graph, a high peak for titanium was obtained, suggesting, as expected, a high concentration of this element.

4. Discussion

In the mechanical tests conducted, in the nanocomposite with 6 wt.%

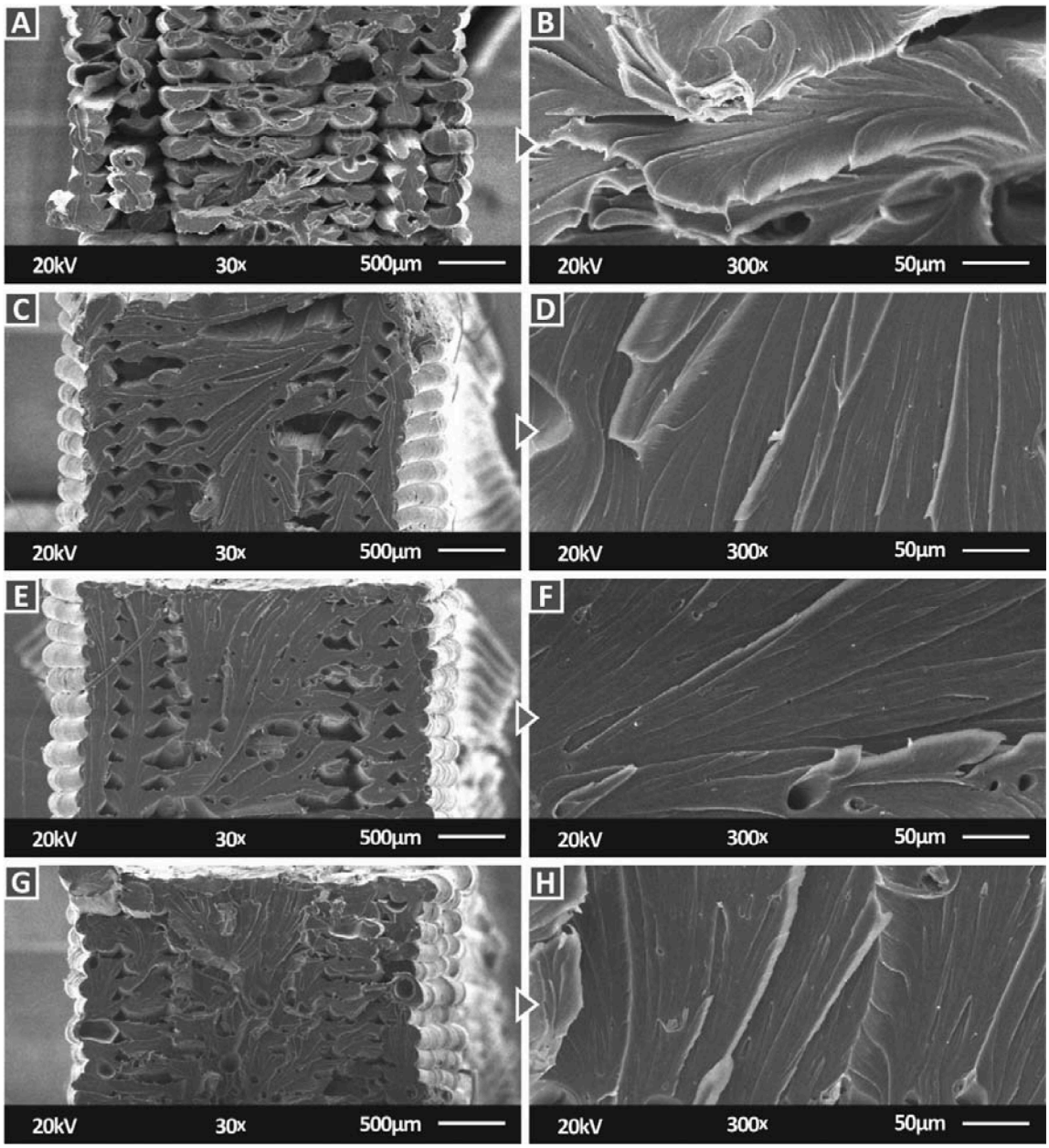

Fig. 15. Fracture surface of the PC/TiN nanocomposites captured with SEM: (A) nanocomposite with 1 wt.% filler concentration at 30 ×, (B) nanocomposite with 1 wt.% filler concentration at 300 ×, (C) nanocomposite with 2 wt.% filler concentration at 30 ×, (D) nanocomposite with 2 wt.% filler concentration at 300 ×, (E) nanocomposite with 3 wt.% filler concentration at 30 ×, (F) nanocomposite with 3 wt.% filler concentration at 300 ×, (G) nanocomposite with 6 wt.% filler concentration at 30 ×, and (H) nanocomposite with 6 wt.% filler concentration at 300 × .

filler loading, the mechanical strength started to decrease, achieving values still improved compared to the pure PC material. This indicates that higher additive concentrations in this range are most likely the saturation point for the PC polymer's filler. The highest mechanical response overall is reported in the nanocomposite with 3 wt.% loading. The mechanical test results are summarized in Fig. 17.

The pure MEX 3D printed PC, as expected, had a lower mechanical response than the bulk material (53 MPa, rather than 60 MPa of the bulk material). This is due to the porosity and anisotropy in the parts caused by the MEX 3D printing process. The introduction of the additive resulted in higher values than that of the pure PC. So, the nanocomposites developed herein can advance 3D printing, further expanding the fields of application of the process. No similar compound is available in the literature to correlate the results of the study for bulk or 3D printed polymers. The filament produced in the study was tested in tensile experiments. These results do not follow a standard, so they cannot be directly compared to the equivalent results of the 3D-printed parts. Still, the fact that all the examples investigated show the same trend of improvement is an indication of the study's credibility.

The pure PC thermal stability was not affected by the introduction of the TiN nano additive, and it was verified that the temperatures used do not cause any degradation effects in the materials. The elements in the nanocomposites were confirmed in the EDS analysis. The morphological characteristics of the specimens were evaluated with SEM, while in the higher magnification images negligible agglomerations were found, even at the nanocomposite with 6 wt.% filler concentration. Finally, the deviation in all the mechanical tests was within a small margin, indicating that a well-distributed NPs network was formed in the nanocomposites of the study, with the methodology followed.

The comparison of the samples with the PC-Pure shows the effect of

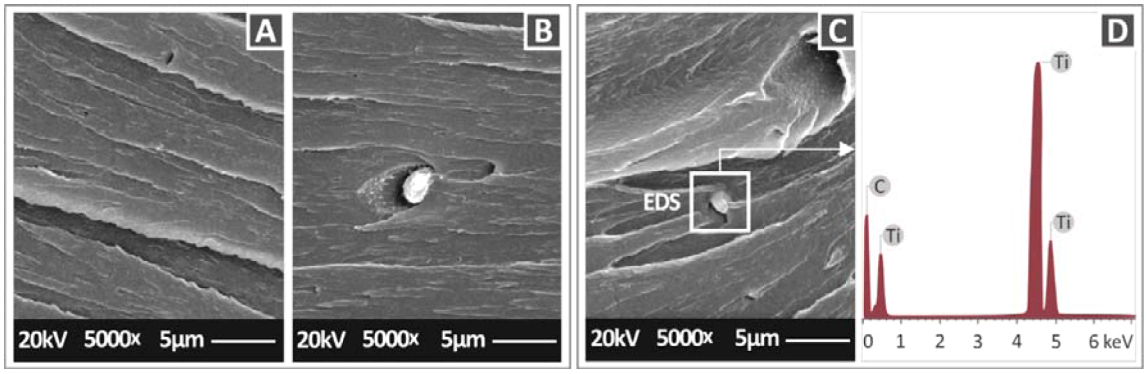

Fig. 16. Fracture surface at 5000 × magnification of the PC/TiN nanocomposites: (A) nanocomposite with 1 wt.% filler concentration (B) nanocomposite with 6 wt.% filler concentration, (C) nanocomposite with 3 wt.% filler concentration, and (D) EDS graph of the nanocomposite with 3 wt.% filler concentration, acquired on the micro-agglomeration depicted in Fig. 16C.

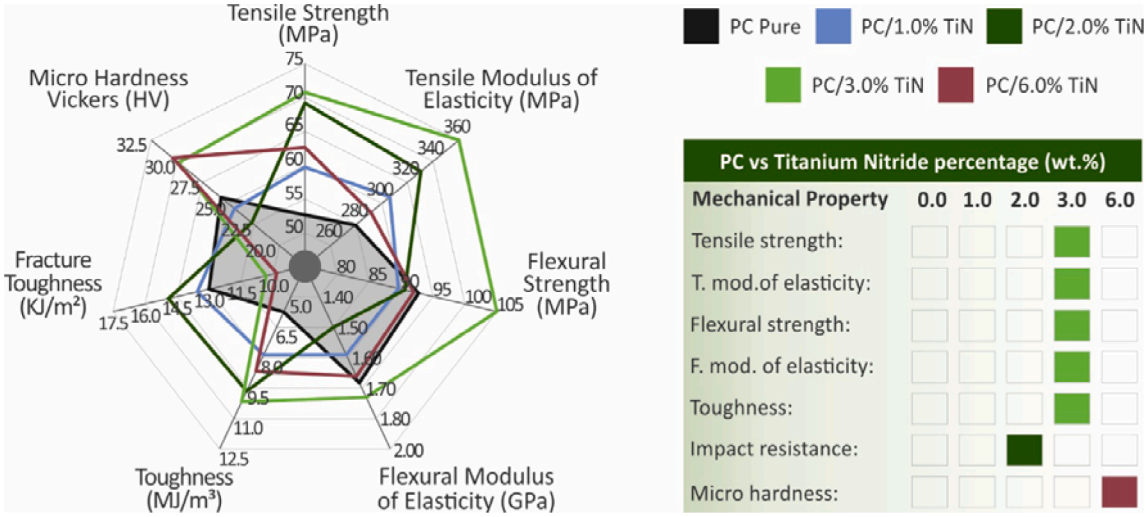

Fig. 17. The mechanical tests' results are summarized in a spider graph. The pure PC is presented in the shaded area. Highest performed material in each test is presented on the right side of the figure.

Table 3
The Raman spectra behavioral differences between the PC-Pure and the TiN samples.

Wavenumber (cm^{-1})	Assignment	Change
607	Unassigned	Decrease of peak for TiN samples
932	C-H in-plane bending	Increase of peak for TiN samples
1498	CH_3 deformation	Decrease of the peak for TiN samples
2934	C—H stretching	Increase of peak for TiN samples

the additive in the Raman peaks. A decrease of the peak for the PC-TiN specimens is depicted at the (607 cm^{-1}), and the CH_3 deformation (1498 cm^{-1}). There is a gradual increase in the C—H plane bending (932 cm^{-1}), and the C—H stretching (2934 cm^{-1}). The aforementioned peaks are presented in Table 3 as well. One interpretation of those results could be that the decrease in the methylated parts of the molecule (1498 cm^{-1}) found in TiN samples, refers to a decrease in the CH3 concentration. The additional increase of C—H peaks (932, 2934 cm^{-1}) could be explained that the bond released from CH_3 has been replaced with C—H bonds. Based on the fact that the dissociation energy of C—H is higher than the one of CH_3, explains the increase in the sample's mechanical properties [59].

Regarding the distribution of the filler in the matrix, apart from the SEM images, in which no agglomerations were found, the deviation in the mechanical tests was within reasonable limits, showing insignificant differences between the samples assessed, which also confirms a similar distribution of the filler in the matrix. As the filler concentration increases, the maximum effect of the filler in the mechanical properties is reached. In higher loading than this, it is expected that the mechanical response starts to decrease until the saturation threshold of the filler in the matrix is reached. This is typical behavior. In this work, loadings up to 6 wt.% were studied, which achieved a lower mechanical response than the nanocomposites with lower filler loading (verifying that the maximum effect of the filler in the matrix was achieved), but still no indication that the 6 wt.% loading is reaching a saturation threshold, can be assumed. Hence, the differences in the morphology presented in the SEM images, are not significant, which is the expected response, when the filler loading reaches the saturation threshold. Identifying the saturation threshold of the filler in the matrix was not the purpose of the work. The work aimed to investigate the effect of the filler in the mechanical response of the matrix and the maximum enhancement was found to be at the nanocomposite with 3 wt.% filler loading.

5. Conclusions

For the first time, in this work, the effect of using TiN as a mechanical reinforcement in the PC polymer for MEX 3D printing was investigated.

TiN in nanopowder form was added to the matrix material with a thermomechanical process at various concentrations, up to 6 wt.%, to evaluate the effect of the additive concentration on the mechanical properties. PC/TiN nanocomposites in a form suitable for MEX 3D printing were prepared, to investigate its performance, exploiting 3D printing advances in an attempt to expand its fields of applications. A thorough mechanical characterization process was followed, and it was verified that TiN can be employed for PC polymer enhancement in MEX 3D printing. Overall, the best performance was achieved by the nanocomposite having a 3 wt.% filler concentration. More specifically, in the 3 wt.% additive nanocomposite the tensile strength was improved by 35% and the Tensile Modulus of Elasticity by 29.0%. It also exhibited enhanced flexural, impact, and microhardness responses.

In addition to mechanical testing, the thermal properties, and the spectroscopic response of all the produced nanocomposites were studied to further comprehend their properties. In all tests, the stability of the materials was verified. No significant processability issues occurred, making the process easily adapted for industrial environments. The main drawback of the 3D printed parts, which is their inferior mechanical response compared to the bulk materials, can be overcome by the development of nanocomposites, such as the ones prepared and studied in this work.

Additionally, the development of such nanocomposites is a cost-effective process, since the only additional cost in the process, is the cost of the filler. For laboratory-scale use, the cost of the specific materials used is roughly 0.04 EUR/gr for the matrix and 0.9 EUR/gr for the TiN additive. For filler concentrations of 3 wt.%, which had the highest enhancement effect in the study, the cost per gram of the nanocomposites is 0.067 EUR (0.04 EUR/gr for the matrix, plus 0.9 × 0.03 EUR/gr for the additive). This increase is not significant in the overall cost of the process. The cost of the raw materials is not the main cost of the process, considering that the masterbatch to filament cost ratio is 1/10, with the same amount of filament cost being ten times the cost of the same amount of raw material. These costs can be further optimized for industrial-scale use. In future work, the process and the filler loading can be further optimized, additional properties can be investigated and the necessary adaptions for industrial-scale use can be determined.

Funding

This research received no external funding.

Data availability

The raw/processed data required to reproduce these findings cannot be shared at this time due to technical or time limitations.

Declaration of Competing Interests

The authors declare that they have no known competing financial interests or personal relationships that could have appeared to influence the work reported in this paper.

Acknowledgments

Authors would like to thank the Institute of Electronic Structure and Laser of the Foundation for Research and Technology-Hellas (IESL-FORTH) and in particular Ms. Aleka Manousaki for taking the SEM images presented in this work, and the Photonic Phononic and Meta-Materials Laboratory for sharing the Raman Instrumentation.

References

[1] X. Mu, et al., High-performance flame-retardant polycarbonate composites: mechanisms investigation and fire-safety evaluation systems establishment, Compos. Part B Eng. 238 (2022), 109873, https://doi.org/10.1016/J.COMPOSITESB.2022.109873.

[2] J. Quereda, et al., Scalable and low-cost fabrication of flexible WS2 photodetectors on polycarbonate, npj Flex. Electron. 6 (2022), https://doi.org/10.1038/s41528-022-00157-9.

[3] P. Chhokkar, et al., Role of energy loss-range profile of heavy ions in tailoring the optical properties of polycarbonate, Opt. Mater. (Amst). 121 (2021), 111617, https://doi.org/10.1016/J.OPTMAT.2021.111617.

[4] W. Tao, Z. Lin, Q. Yuan, P. Gong, Estimation of effective thickness of cyclopore polycarbonate membrane by scanning electrochemical impedance microscopy, J. Electroanal. Chem. 905 (2022), 115974, https://doi.org/10.1016/J.JELECHEM.2021.115974.

[5] A.S. Budiman, et al., Enabling lightweight polycarbonate-polycarbonate (PC-PC) photovoltaics module technology – Enhancing integration of silicon solar cells into aesthetic design for greener building and urban structures, Sol. Energy 235 (2022) 129–139, https://doi.org/10.1016/J.SOLENER.2022.02.018.

[6] K. Pan, et al., Preparation of photo-crosslinked aliphatic polycarbonate coatings with predictable degradation behavior on magnesium-alloy stents by electrophoretic deposition, Chem. Eng. J. 427 (2022), 131596, https://doi.org/10.1016/J.CEJ.2021.131596.

[7] G. Allen, D.C.W. Morley, T. Williams, The impact strength of polycarbonate, J. Mater. Sci. 8 (1973) 1449–1452, https://doi.org/10.1007/BF00551669.

[8] T. Krausz, D.A. Serban, R.M. Negru, A.G. Radu, L. Marsavina, The effect of strain rate and temperature on the mechanical properties of polycarbonate composites, Mater. Today Proc. 45 (2021) 4211–4215, https://doi.org/10.1016/J.MATPR.2020.12.121.

[9] A. Eitan, F.T. Fisher, R. Andrews, L.C. Brinson, L.S. Schadler, Reinforcement mechanisms in MWCNT-filled polycarbonate, Compos. Sci. Technol. 66 (2006) 1162–1173, https://doi.org/10.1016/J.COMPSCITECH.2005.10.004.

[10] A. Davis, J.H. Golden, Stability of Polycarbonate, J. Macromol. Sci. Part C 3 (1969) 49–68, https://doi.org/10.1080/15583726908545896.

[11] B. Koker, et al., Enhanced interlayer strength and thermal stability via dual material filament for material extrusion additive manufacturing, Addit. Manuf. 55 (2022), 102807, https://doi.org/10.1016/J.ADDMA.2022.102807.

[12] Q. Qian, et al., 3D reactive inkjet printing of bisphenol A-polycarbonate, Addit. Manuf. 54 (2022), 102745, https://doi.org/10.1016/J.ADDMA.2022.102745.

[13] Z. Liu, J. Zhan, M. Fard, J.L. Davy, Acoustic properties of a porous polycarbonate material produced by additive manufacturing, Mater. Lett. 181 (2016) 296–299, https://doi.org/10.1016/J.MATLET.2016.06.045.

[14] S.J. Park, et al., 3D printing of bio-based polycarbonate and its potential applications in ecofriendly indoor manufacturing, Addit. Manuf. 31 (2020), 100974, https://doi.org/10.1016/j.addma.2019.100974.

[15] O. Takeda, K. Suzuki, R. Nakajima, K. Maeda, T. Gonjo, N. Fujii, Evaluation of polycarbonate additive manufacturing molds for autoclave molding, Res. Sq. (2022) 1–11, https://doi.org/10.21203/rs.3.rs-1433414/v1. License.

[16] J.R. Ai, B.D. Vogt, Size and print path effects on mechanical properties of material extrusion 3D printed plastics, Prog. Addit. Manuf. (2022), https://doi.org/10.1007/s40964-022-00275-w.

[17] N. Vidakis, et al., Strain rate sensitivity of polycarbonate and thermoplastic polyurethane for various 3D printing temperatures and layer heights, Polymers (Basel) 13 (2021) 2752, https://doi.org/10.3390/polym13162752.

[18] N. Dialami, I. Rivet, M. Cervera, M. Chiumenti, Computational characterization of polymeric materials 3D-printed via fused filament fabrication, Mech. Adv. Mater. Struct. 0 (2022) 1–11, https://doi.org/10.1080/15376494.2022.2032496.

[19] N. Vidakis, M. Petousis, J.D. Kechagias, A comprehensive investigation of the 3D printing parameters' effects on the mechanical response of polycarbonate in fused filament fabrication, Prog. Addit. Manuf. (2022), https://doi.org/10.1007/s40964-021-00258-3.

[20] P. Stavropoulos, A. Papacharalampoloulos, K. Tzimanis, Design and implementation of a digital twin platform for AM processes, Procedia CIRP 104 (2021) 1722–1727, https://doi.org/10.1016/j.procir.2021.11.290.

[21] T. Nancharaiah, Optimization of Process Parameters in FDM Process Using Design of Experiments 2 (2011) 100–102.

[22] T. Arai, M. Kawaji, Thermal performance and flow characteristics in additive manufactured polycarbonate pulsating heat pipes with Novec 7000, Appl. Therm. Eng. (2021), 117273, https://doi.org/10.1016/j.applthermaleng.2021.117273.

[23] N. Vidakis, M. Petousis, S. Grammatikos, V. Papadakis, A. Korlos, N. Mountakis, High performance polycarbonate nanocomposites mechanically boosted with titanium carbide in material extrusion additive manufacturing, Nanomaterials 12 (2022) 1068, https://doi.org/10.3390/nano12071068.

[24] N. Vidakis, M. Petousis, E. Velidakis, M. Spiridaki, J. Kechagias, Mechanical performance of fused filament fabricated and 3D-printed polycarbonate polymer and polycarbonate/cellulose nanofiber nanocomposites, Fibers 9 (2021) 74, https://doi.org/10.3390/fib9110074.

[25] D. Kodali, C.O. Umerah, and V.K. Rangari, Fabrication and characterization of polycarbonate-silica filaments for 3D printing applications, 55 (2021) 4575–4584. doi: 10.1177/00219983211044748.

[26] M.R. Zakaria, H. Md Akil, M.F. Omar, M.H. Abdul Kudus, F.N.A. Mohd Sabri, M.M. A.B. Abdullah, Enhancement of mechanical and thermal properties of carbon fiber epoxy composite laminates reinforced with carbon nanotubes interlayer using electrospray deposition, Compos. Part C Open Access (2020) 3, https://doi.org/10.1016/j.jcomc.2020.100075.

[27] A. Bifulco, et al., Improving flame retardancy of in-situ silica-epoxy nanocomposites cured with aliphatic hardener: combined effect of DOPO-based flame-retardant and melamine, Compos. Part C Open Access 2 (2020) 0–37, https://doi.org/10.1016/j.jcomc.2020.100022.

[28] Z. Viskadourakis, M. Sevastaki, G. Kenanakis, 3D structured nanocomposites by FDM process: a novel approach for large-scale photocatalytic applications, Appl.

Phys. A Mater. Sci. Process. 124 (2018) 0, https://doi.org/10.1007/s00339-018-2014-6.
[29] N. Maqsood, M. Rimašauskas, Characterization of carbon fiber reinforced PLA composites manufactured by fused deposition modeling, Compos. Part C Open Access 4 (2021), https://doi.org/10.1016/j.jcomc.2021.100112.
[30] N. Vidakis, A. Maniadi, M. Petousis, M. Vamvakaki, G. Kenanakis, E. Koudoumas, Mechanical and electrical properties investigation of 3D-printed acrylonitrile–butadiene–styrene graphene and carbon nanocomposites, J. Mater. Eng. Perform. 29 (2020) 1909–1918, https://doi.org/10.1007/s11665-020-04689-x.
[31] N. Vidakis, M. Petousis, E. Velidakis, M. Liebscher, L. Tzounis, Three-dimensional printed antimicrobial objects of polylactic acid (PLA)-silver nanoparticle nanocomposite filaments produced by an in-situ reduction reactive melt mixing process, Biomimetics 5 (2020) 42, https://doi.org/10.3390/biomimetics5030042.
[32] and L.T. Nectarios Vidakis, Markos Petousis, Athena Maniadi, Marco Liebscher, Mechanical properties of 3D-printed acrylonitrile–butadiene–styrene TiO2 and ATO nanocomposites, Polymers (Basel) 13 (2021) 123–129. doi: 0.3390/polym12071589.
[33] N. Vidakis, et al., The mechanical and physical properties of 3D-Printed materials composed of ABS-ZnO nanocomposites and ABS-ZnO microcomposites, Micromachines (Basel) 11 (2020) 1–20, https://doi.org/10.3390/mi11060615.
[34] K. Anyfantis, P. Stavropoulos, P. Foteinopoulos, G. Chryssolouris, An approach for the design of multi-material mechanical components, Proc. Inst. Mech. Eng. Part B J. Eng. Manuf. 233 (2019) 960–974, https://doi.org/10.1177/0954405418763995.
[35] S.S. Babu, L. Love, R. Dehoff, W. Peter, T.R. Watkins, S. Pannala, Additive manufacturing of materials: opportunities and challenges, MRS Bull. 40 (2015) 1154–1161, https://doi.org/10.1557/mrs.2015.234.
[36] H.Z. Wu, T.C. Chou, A. Mishra, D.R. Anderson, J.K. Lampert, S.C. Gujrathi, Characterization of titanium nitride thin films, Thin Solid Films 191 (1990) 55–67, https://doi.org/10.1016/0040-6090(90)90274-H.
[37] E. Santecchia, A.M.S. Hamouda, F. Musharavati, E. Zalnezhad, M. Cabibbo, S. Spigarelli, Wear resistance investigation of titanium nitride-based coatings, Ceram. Int. 41 (2015) 10349–10379, https://doi.org/10.1016/j.ceramint.2015.04.152.
[38] R. Machunze, G.C.A.M. Janssen, Stress and strain in titanium nitride thin films, Thin Solid Films 517 (2009) 5888–5893, https://doi.org/10.1016/j.tsf.2009.04.020.
[39] R.P. Van Hove, I.N. Sierevelt, B.J. Van Royen, P.A. Nolte, Titanium-nitride coating of orthopaedic implants: a review of the literature, Biomed Res. Int. 2015 (2015), https://doi.org/10.1155/2015/485975.
[40] Q. Jiao, T. Zhou, N. Zhang, S. Liu, Q. Huang, and W. Bi, High-surface-area titanium nitride nanosheets as zinc anode coating for dendrite-free rechargeable aqueous batteries, (2022) 1–8.
[41] P. Song, B. Liu, H. Qiu, X. Shi, D. Cao, J. Gu, MXenes for polymer matrix electromagnetic interference shielding composites: a review, Compos. Commun. 24 (2021), 100653, https://doi.org/10.1016/j.coco.2021.100653.
[42] N. Iizuka, J. Fukushima, Y. Hayashi, H. Takizawa, Microwave-assisted titanium nitride coating processing using nitride powders in ambient atmosphere, J. Alloys Compd. 908 (2022), 164606, https://doi.org/10.1016/j.jallcom.2022.164606.
[43] K.-G.-G.C. De Silva, M. Finale, S. Chowdhury, Plasmon mediated deposition of Ni on Titanium Nitride nanoparticles: applications in enhanced photoreduction of bicarbonate, Mater. Res. Bull. (2022), 111834, https://doi.org/10.1016/j.materresbull.2022.111834.
[44] P. Patsalas, N. Kalfagiannis, S. Kassavetis, Optical properties and plasmonic performance of titanium nitride, Materials (Basel) 8 (2015) 3128–3154, https://doi.org/10.3390/ma8063128.
[45] J.A. Briggs, et al., Temperature-dependent optical properties of titanium nitride, Appl. Phys. Lett. 110 (2017), https://doi.org/10.1063/1.4977840.
[46] T.D.S. Gururaj, V. Naik, Jeremy L. Schroeder, Xingjie Ni, Alexander V. Kildishev, A. Boltasseva, Titanium nitride as a plasmonic material for visible and near-infrared wavelengths, Opt. Soc. Am. OCIS 2 (2012) 478–489.
[47] B.S. Simpkins, S.I. Maximenko, and O. Baturina, Potential of TiN /GaN heterostructures for hot carrier generation and collection, (2022).
[48] Y. Zhang, H. Sahasrabudhe, A. Bandyopadhyay, Additive manufacturing of Ti-Si-N ceramic coatings on titanium, Appl. Surf. Sci. 346 (2015) 428–437, https://doi.org/10.1016/j.apsusc.2015.03.184.
[49] T.C. Dzogbewu, W.B. du Preez, Additive manufacturing of titanium-based implants with metal-based antimicrobial agents, Metals (Basel) 11 (2021) 1–12, https://doi.org/10.3390/met11030453.
[50] U. Guler, et al., Plasmonic titanium nitride nanostructures via nitridation of nanopatterned titanium dioxide, Adv. Opt. Mater. 5 (2017), https://doi.org/10.1002/adom.201600717.
[51] P. Pedrosa, et al., TiN x coated polycarbonate for bio-electrode applications, Corros. Sci. 56 (2012) 49–57, https://doi.org/10.1016/j.corsci.2011.11.008.
[52] C. Chaiwong, D.R. McKenzie, M.M.M. Bilek, Cracking of titanium nitride films grown on polycarbonate, Surf. Coatings Technol. 201 (2007) 5596–5600, https://doi.org/10.1016/j.surfcoat.2006.07.200.
[53] M. Samykano, S.K. Selvamani, K. Kadirgama, W.K. Ngui, G. Kanagaraj, K. Sudhakar, Mechanical property of FDM printed ABS: influence of printing parameters, Int. J. Adv. Manuf. Technol. 102 (2019) 2779–2796, https://doi.org/10.1007/s00170-019-03313-0.
[54] P. Foteinopoulos, V. Esnault, G. Komineas, A. Papacharalampopoulos, P. Stavropoulos, Cement-based additive manufacturing: experimental investigation of process quality, Int. J. Adv. Manuf. Technol. 106 (2020) 4815–4826, https://doi.org/10.1007/s00170-020-04978-8.
[55] B.H. Stuart, Temperature studies of polycarbonate using Fourier transform Raman spectroscopy, Polym. Bull. 36 (1996) 341–346, https://doi.org/10.1007/BF00319235.
[56] M. Makarem, et al., Probing cellulose structures with vibrational spectroscopy, Cellulose 26 (2019) 35–79, https://doi.org/10.1007/s10570-018-2199-z.
[57] C. Zimmerer, et al., Nondestructive characterization of the polycarbonate - octadecylamine interface by surface enhanced Raman spectroscopy, Polym. Test. 73 (2019) 152–158, https://doi.org/10.1016/j.polymertesting.2018.11.023.
[58] V. Resta, G. Quarta, M. Lomascolo, L. Maruccio, L. Calcagnile, Raman and Photoluminescence spectroscopy of polycarbonate matrices irradiated with different energy 28Si+ ions, Vacuum 116 (2015) 82–89, https://doi.org/10.1016/j.vacuum.2015.03.005.
[59] K. May, B.V. Unterreiner, S. Dapprich, R. Ahlrichs, Structures and C-H bond energies of hydrogenated polycyclic aromatic hydrocarbons, Phys. Chem. Chem. Phys. 2 (2000) 5089–5092, https://doi.org/10.1039/b005597m.